

# Track-finding efficiency at Belle II

Reshma Menon R

Registration No: 19PH05009



School of Basic Sciences, Indian Institute of Technology  
Bhubaneswar, Jatni, Khurda, Odisha, 752050, India

Supervisor: Dr. Seema Bahinipati

# Contents

<b>1</b>	<b>Super KEKB and Belle II</b>	<b>5</b>
<b>2</b>	<b>The Belle II detector</b>	<b>6</b>
<b>3</b>	<b>Analysis tool:ROOT</b>	<b>8</b>
<b>4</b>	<b>Relative Tracking Efficiency of slow pions</b>	<b>9</b>
4.1	Introduction . . . . .	9
4.2	Method . . . . .	9
4.3	Data and Monte Carlo samples . . . . .	10
4.4	Event selection . . . . .	10
4.5	Fit Procedure . . . . .	11
4.6	Results for $\bar{D}^0 \rightarrow K^- \pi^+ \pi^- \pi^+$ mode . . . . .	11
4.7	Results for $\bar{D}^0 \rightarrow K^- \pi^+$ mode . . . . .	13
4.8	Final results: . . . . .	15
4.9	Conclusions: . . . . .	15
<b>5</b>	<b>Details of the Silicon Vertex Detector(SVD)</b>	<b>16</b>
5.1	SVD Outer Layout: . . . . .	16
5.2	SVD sensors and readout electronics . . . . .	18
5.3	SVD Ladders . . . . .	18
5.4	Design basics of a silicon micro-strip sensors: . . . . .	19
<b>6</b>	<b>Double Sided Silicon Sensors (DSSD's)</b>	<b>20</b>

6.1	Working Principle: . . . . .	20
<b>7</b>	<b>Electrical Test Procedures</b>	<b>22</b>
7.1	Defect Types: . . . . .	23
<b>8</b>	<b>Software Setup:</b>	<b>25</b>
8.1	Package Content: . . . . .	25
<b>9</b>	<b>SVD aDefectFinder analysis</b>	<b>26</b>
9.1	aDF analysis of 2021-02-03 run; Exp 15, Run 285 . . . . .	26
9.2	aDF analysis of local run with Vsep=-0.8V (taken on Feb 1) + vsep scan (taken on Feb 3);Exp 15,Run 223 . . . . .	29
9.3	aDF analysis of 2020-11-11 run;Exp 14 ,Run 1028 . . . . .	31
9.4	aDF analysis of 2020-11-18 run;Exp 14,Run 1241 . . . . .	33
9.5	aDF analysis of 2021-03-23 run;Exp 16 ,Run 1168 . . . . .	35
	<b>Bibliography</b>	<b>37</b>

# Abstract

## Track-finding efficiency at Belle II

Reshma Menon R

Supervisor:Dr. Seema Bahinipati

May 2021

Track finding efficiency is a vital input to various sources of systematic uncertainties in analyses involving charged particles. Method to calculate tracking efficiency for hadrons is different than that for muons due their decays and interactions with the material of the detector. Therefore, here we describe a method of estimating the relative tracking efficiency of slow pions in data compared to simulation by focusing on  $B^0 \rightarrow D^{*-}\pi^+$  decay where the  $D^{*-}$  further decays to  $\bar{D}^0\pi^-$ . Owing to its limited phase space, the pion from  $D^*$  decay is traditionally referred as slow-pion due to a small mass difference between the  $D^*$  and  $\bar{D}^0$ . The main aim of this project is to determine the relative tracking efficiency of this slow pion in data and simulation by measuring the efficiency corrected yield ratio for  $\bar{D}^0 \rightarrow K^-\pi^+\pi^-\pi^+$  mode relative to that for the two-body decay  $\bar{D}^0 \rightarrow K^-\pi^+$ .

Besides this, the project also aims at maintaining the health of the sub-detector: Silicon Vertex Detector (SVD) at Belle II. The main purpose of SVD is to determine the decay vertices and to precisely measure the momentum of charged particles. Regular electrical tests are conducted to check the correct functionality and to identify the possible defects of the electrically active components. Here we try to understand, classify and analyse the electrical defects of the SVD sensors. We also aim to understand the effect of radiation damage in increasing the number of defects (majorly pinholes) in a sensor. These defects obtained on electrical characterisation of SVD sensors need to be fixed at regular intervals in order to have precise measurements.

## **Acknowledgements**

Throughout this project, I have received a great deal of support and assistance.

I would first like to thank my supervisor, Dr. Seema Bahinipati for her constant encouragement and support throughout this work. She has been a source of motivation and inspiration. It was an amazing learning experience working with her.

I would like to acknowledge our EHEP group for their support and guidance. Our weekly group meetings and discussions have helped me develop my analysis skills.

I would also like to thank my parents for being my strength through all the thick and thins. Their unconditional love and encouragement has been a source of motivation throughout.

# Chapter 1

## Super KEKB and Belle II

From 1998 to 2010 [1], KEK, the Japanese High-Energy Accelerator Research Organisation, operated KEKB which is an asymmetric electron-positron collider. The beam energies are such that in the collisions mainly B-mesons are produced and is therefore known as a B factory experiment. The Belle experiment analyses the characteristics of pairs of B meson and anti-B-mesons and confirms the effect of CP-violation which is one of the origins for the observed dominance of matter over anti-matter in our universe. The measured level of CP-violation is insufficient to briefly explain the actual asymmetry. One needs a deeper understanding and clarity of this phenomena.

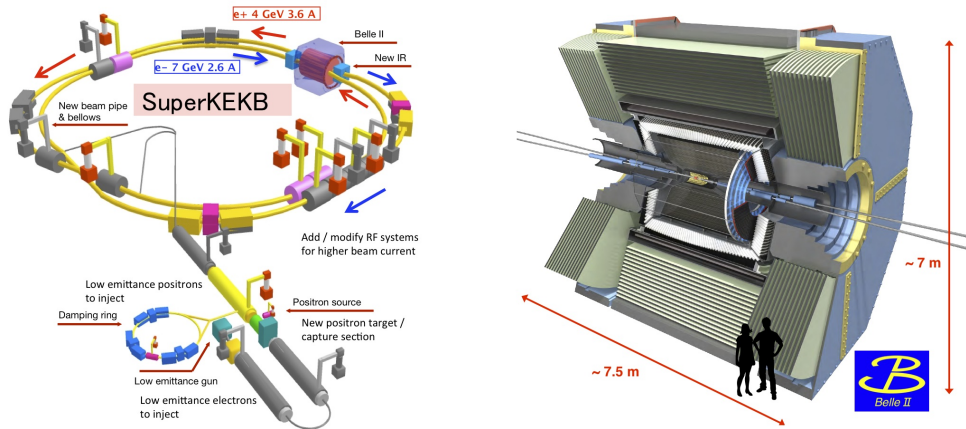


Figure 1.1: Super KEKB and Belle II [1].

SuperKEKB is the upgraded version of KEKB with 40 times higher luminosity. The accelerator achieved "first turns" in February 2016 and first collision on 26 April, 2018. On 15th June 2020 at 20:34, SuperKEKB achieved the world's highest instantaneous luminosity for a colliding-beam accelerator, setting a record of  $2.22 \times 10^{34} \text{ cm}^{-2} \text{ s}^{-1}$ .

## Chapter 2

# The Belle II detector

The former Belle experiment was a particle detector designed to precisely measure the decay products of B mesons [1]. The decay cascade ends up in particles long-lived enough to enter the detector to be measured. The detector measures each of these “final state” particles with high precision, in order to have a chance of reconstructing the primary interaction.

### Upgradation to Belle II:

With the new SuperKEKB collider, the Belle detector also got upgraded. The 40-fold increase in luminosity created considerable challenges especially to the innermost detector systems. The goal is to maintain the detector performance similar to the former Belle experiment.



Figure 2.1: Logo of the Belle II collaboration [1].

The main components of the Belle II detector are:

1. Vertex Detector (VXD): The Vertex Detector is the innermost sub-detector of Belle II which is designed to perform online and offline tracking of charged particles with a central role in producing the vertex resolution required to perform the Belle II physics program. Four layers of double sided-silicon strip detectors (SVD) and two layers of pixel detectors(PXD) integrated to construct the 6-layer tracking device.The operating principle of the two sub-detectors is different.
2. Central Drift Chamber (CDC): A large gaseous detector acts as main tracking device, measuring the tracks and momenta of the decay products.
3. Silica-Aerogel Cherenkov Counter (ACC): Used for particle identification, mainly used to distinguish between pions and kaons.
4. Time-of-Flight Counters (TOF): Uses plastic scintillators to perform particle identification by measuring the particle's velocity, and provides precise timing signals for triggering.
5. Electromagnetical Calorimeter (ECL): Detects photons and measures their energy and position with thallium-doped caesium iodide crystals.
6. Kaon and Muon Detection System (KLM): This outermost system detects muons and long-lived neutral kaons, and distinguishes between them.This is done by using alternating layers of glass-electrode resistive plate counters and iron plates.
7. Superconducting Solenoid: Provides a homogeneous magnetic field of 1.5 T along the beam axis.

Other essential tasks for the detector:

1. To record collision events of interest,a fast and a reliable trigger (TRG) and data acquisition system (DAQ) is important.
2. A stable operation of superconducting solenoid magnet.
3. a globally-distributed computing and data-storage system and organized effort on various levels of software that work on the computer (Soft/Comp).
4. Components arranged around the interaction point(IR) such as beam pipe and final focussing magnets,which directly impacts the beam background amount.
5. An integrated effort on the mechanical structure design (STR).

## Chapter 3

# Analysis tool:ROOT

ROOT is an object oriented programming platform developed by CERN, based on C++ but is also integrated with R and Python [4]. It was originally developed for handling large amount of data in Particle Physics experiments and include many libraries .Nowadays it is used in many different fields like astronomy and data mining as well.Its main functionalities includes machine learning(TMVA), visualization, curve fitting etc.

Some packages include-

1. Histograms to view and analyze distributions and function.
2. Fitting curves with appropriate probability distribution functions.
3. 3D visualization
4. Interfacing Monte Carlo event generation.
5. Four vector computations.
6. Supports formats like PDF, PNG, LATEX etc.
7. Standard Mathematical functions.

The most widely used data-structure in ROOT are "trees", with substructure as branches and leaves. Accessing of the data becomes quite easy as they are indexed which avoids memory allocation problems associated with object creation and allows tree to act as a light-weight container for raw data.

ROOT's high computing efficiency, makes it efficient to process data from LHC experiments. It is mainly used in data analysis in particle physics experiment and current experiment plots and results are obtained mostly using ROOT. When CMS and ATLAS presented the status of Standard Model Higgs search,all the plots were obtained using ROOT.

## Chapter 4

# Relative Tracking Efficiency of slow pions

### 4.1 Introduction

Track finding efficiency is a vital input to various sources of systematic uncertainties in analyses involving charged particles. Method to calculate tracking efficiency for hadrons is different than that for muons due their decays and interactions with the material of the detector. An earlier measurement of the relative tracking efficiency of pions in the low momentum region of 50-320 MeV with a luminosity of  $57.9 \text{ fb}^{-1}$ , was performed by the Belle II group [5]. Our aim here is to perform an important validation study for their slow pion tracking efficiency numbers.

### 4.2 Method

The relative efficiency of reconstructing pion tracks in data and simulation can be determined by measuring the ratio of neutral charm-meson decays to final states of four or two charged particles [3]. Specifically, we measure the production rate for  $\bar{D}^0 \rightarrow K^- \pi^+ \pi^- \pi^+$  relative to that for the two-body decay  $\bar{D}^0 \rightarrow K^- \pi^+$  in both data and simulated samples. Assuming that the kinematic properties of the two decay modes are properly reproduced in the simulation, the ratio of efficiency-corrected signal yields,

$$R = \frac{N_{K3\pi}}{N_{K\pi}} \cdot \frac{\epsilon_{K\pi}}{\epsilon_{K3\pi}}$$

should be equal to the world-average ratio of branching fractions  $R(\text{PDG})$  [6]. The relative tracking efficiency for pions in data and simulation can then be estimated as

$$\frac{\epsilon(\text{data})}{\epsilon(\text{MC})} = \sqrt{\frac{R}{R(\text{PDG})}}$$

### 4.3 Data and Monte Carlo samples

We generate 200K signal MC events using release-05-01-03. Beam background is not taken into account while generating these events. Since signal MC is used only to determine the  $M_{bc}$  shape which is later used for fitting data events, it is not crucial to have beam background overlaying.

#### Sample details [5]:

1. MC: MC13a [100 fb<sup>-1</sup> ]
2. Data: bucket 9,10,11,14,15 and proc11 [57.9 fb<sup>-1</sup> ], hlt hadron and good runs.

### 4.4 Event selection

The following criteria are used to select candidate events [5]:

1. Charged tracks are selected after applying a selection criteria  $|dr| < 1\text{cm}$  and  $|dz| < 3\text{cm}$  where  $dr$  and  $dz$  are referred as the distance of closest approach in the transverse and longitudinal directions, respectively.
2. Kaon ID:  $L_K/(L_K + L_\pi) > 0.6$  , where  $L_K$  and  $L_\pi$  is the likelihood for kaon and pion respectively.
3. Pion ID:  $L_\pi/(L_K + L_\pi) > 0.6$ .
4. We apply  $\bar{D}^0$  mass window,  $|M_{D^0} - M_{D^0}^{PDG}| < 40\text{ MeV}/c^2$  to suppress combinatorial background.
5. Further we constrained  $D^*$  momentum to be less than 2.5 GeV/c to ensure the event coming from  $B^0 \bar{B}^0$ .
6.  $0.143 < \Delta M = M_{D^*} - M_{D^0} < 0.147\text{ GeV}/c^2$  ,to suppress combinatorial background.
7. Beam-energy-constrained mass,  $M_{bc}$  should be within 5.20 to 5.29 GeV/c<sup>2</sup> .
8.  $|\Delta E| < 0.04\text{ GeV}$  where  $\Delta E = \sum E_i - E_{beam}$ .  $E_{beam}$  here is the beam energy.
9. Number of CDC hits  $> 0$ .
10. The main background in our analysis is from the  $e^+ e^- \rightarrow q\bar{q}$  (q = u, d, s or c) continuum events. This background is suppressed by utilizing an event topology variable (R2), which is different for  $B^0 \bar{B}^0$  events. We maintain  $R2 < 0.3$ .

## 4.5 Fit Procedure

We first fit  $M_{bc}$  from signal MC sample to extract yield after applying all the selection criteria mentioned above. This fit will give us efficiency value. Once this is done, we move towards the data sample by maintaining same signal parameters as in MC. We fit  $M_{bc}$  in data sample by selecting an appropriate PDF for the background. This fit will give us yield which is then directly used to determine R.

## 4.6 Results for $\bar{D}^0 \rightarrow K^- \pi^+ \pi^- \pi^+$ mode

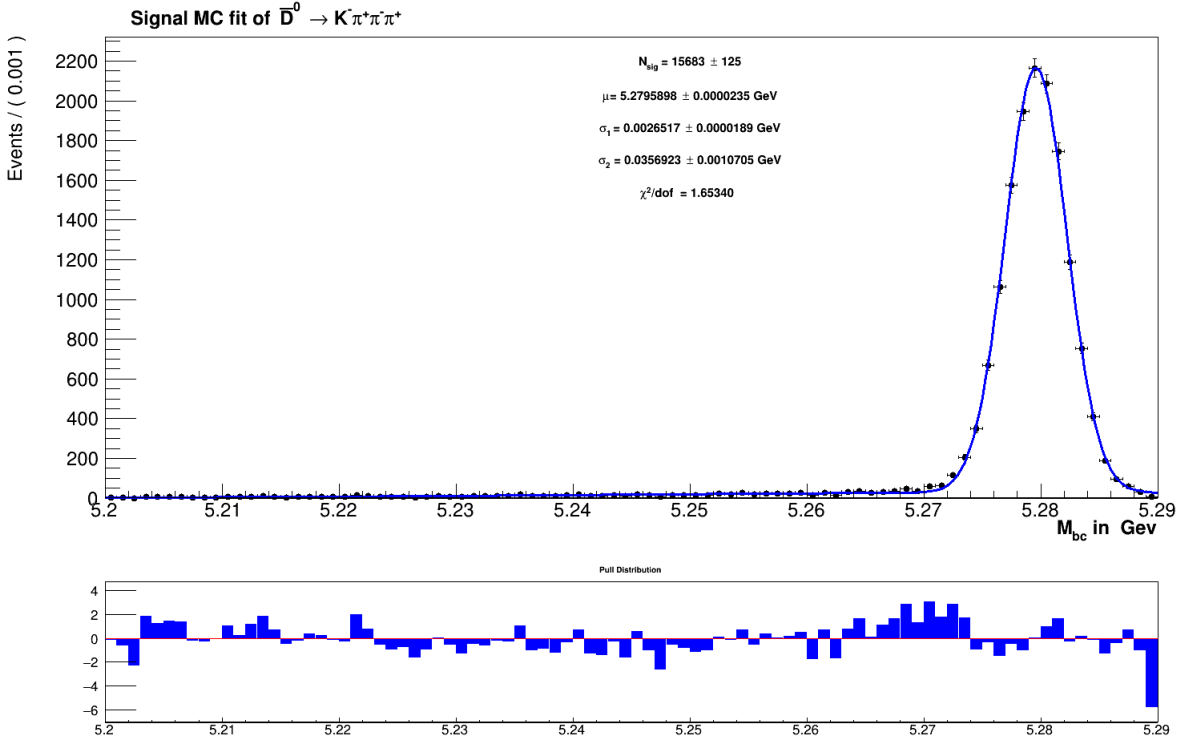


Fig 4.1: Plot shows the fitted distribution of  $M_{bc}$  for  $\bar{D}^0 \rightarrow K^- \pi^+ \pi^- \pi^+$  mode in signal MC. Data points are shown by points with error bars. Total fit PDF is shown by solid blue curve.

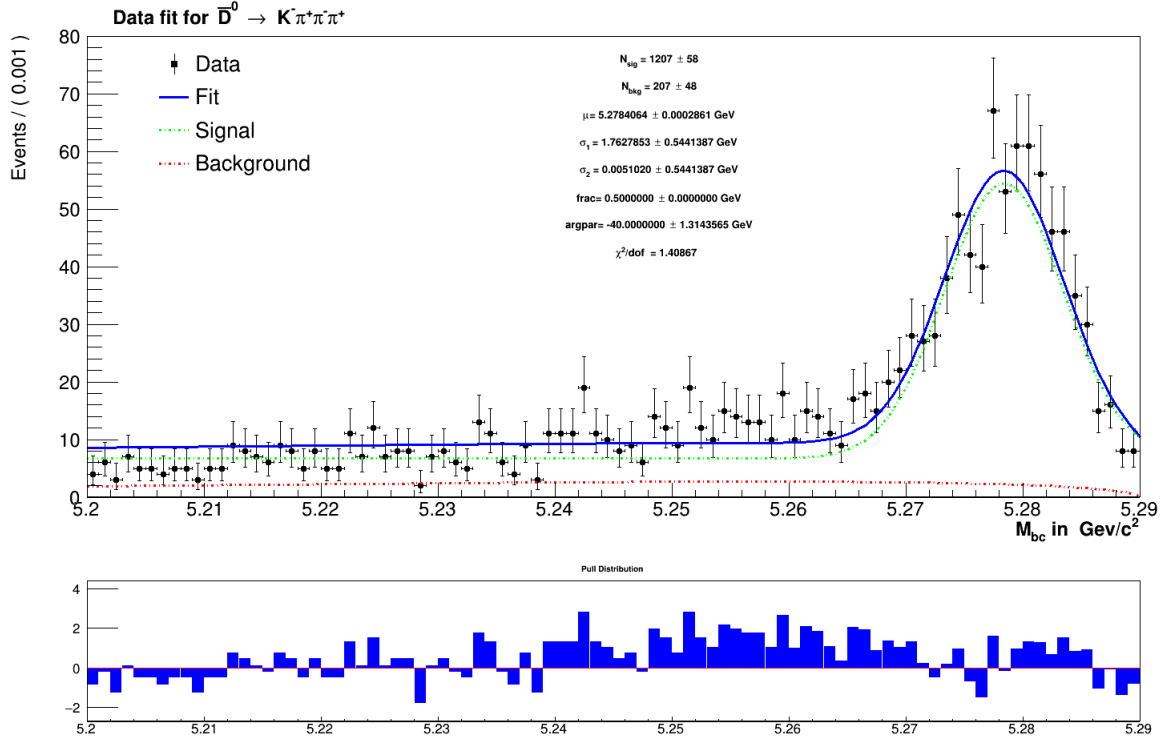


Fig 4.2: Plot shows the fitted distribution of  $M_{bc}$  for  $\bar{D}^0 \rightarrow K^- \pi^+ \pi^- \pi^+$  mode for data sample .

PDF used for signal	Double Gaussian
PDF used for background	Argus Function(one parameter fixed at 5.29)
Efficiency	7.84 %
Data yield	$1414 \pm 75$

Table 4.1: PDF's used and final results of  $M_{bc}$  fit for  $\bar{D}^0 \rightarrow K^- \pi^+ \pi^- \pi^+$  mode.

## 4.7 Results for $\bar{D}^0 \rightarrow K^- \pi^+$ mode

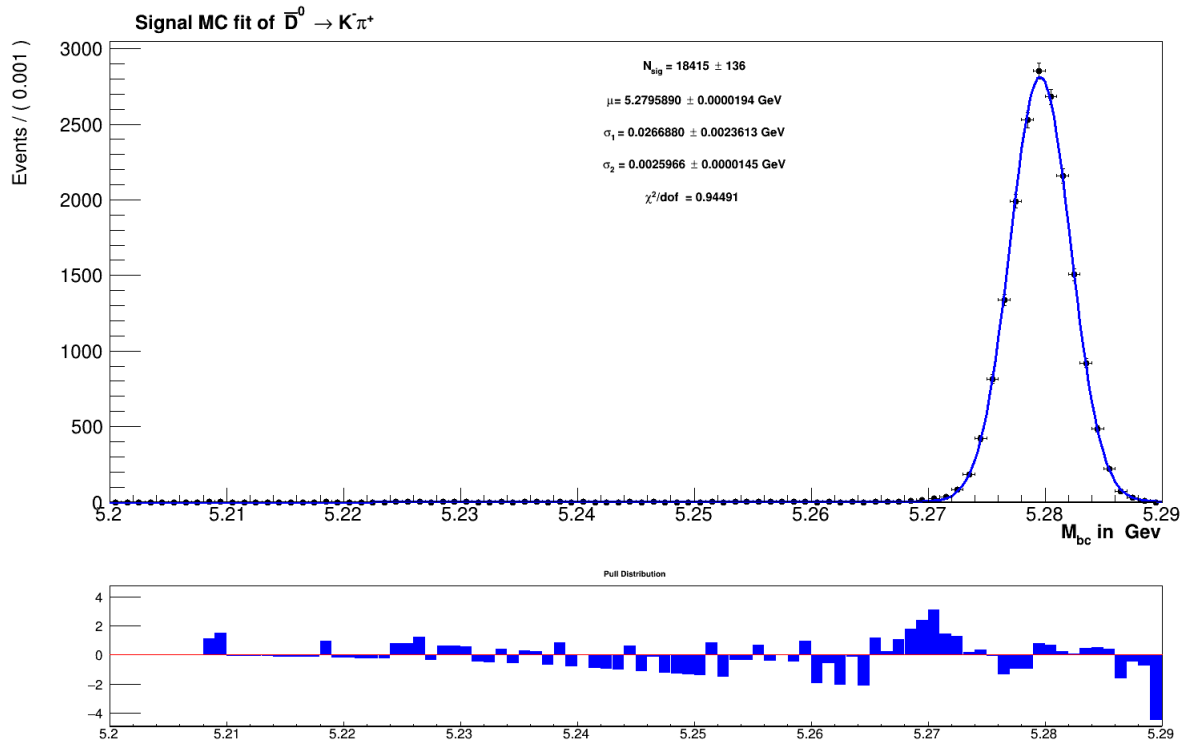


Fig 4.3:Plot shows the fitted distribution of  $M_{bc}$  for  $\bar{D}^0 \rightarrow K^- \pi^+$  mode in signal MC.Data points are shown by points with error bars.Total fit PDF is shown by solid blue curve.

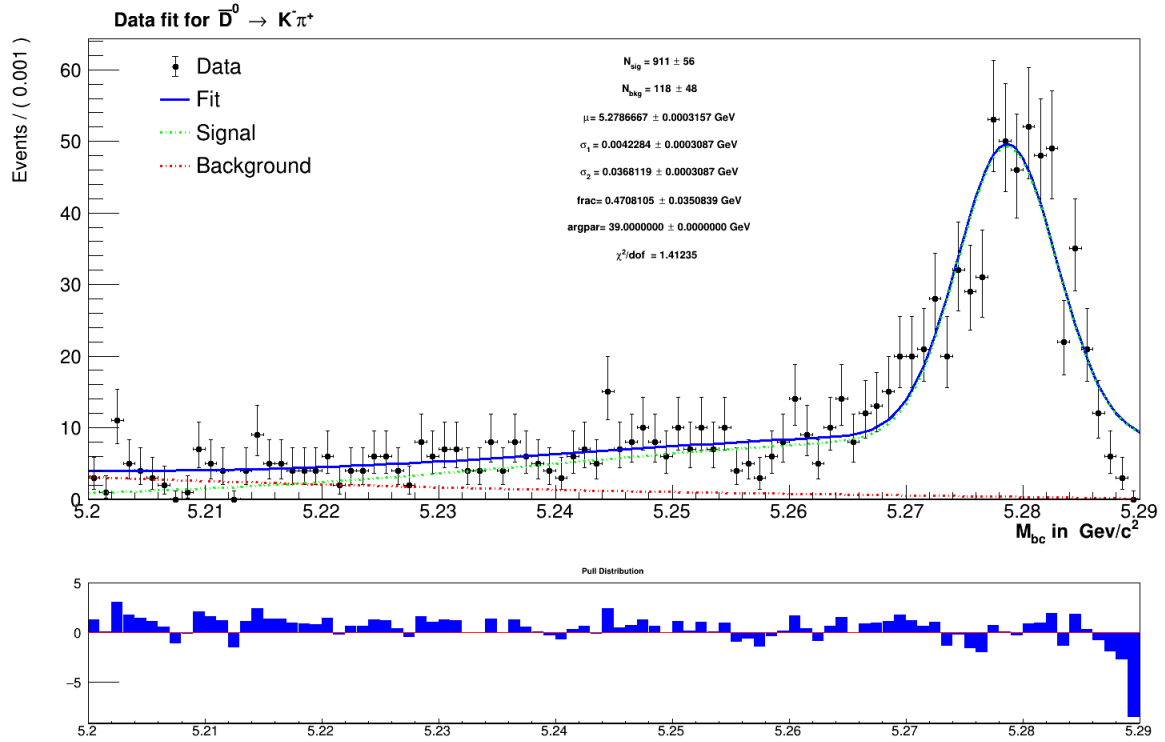


Fig 4.4: Plot shows the fitted distribution of  $M_{bc}$  for  $\bar{D}^0 \rightarrow K^- \pi^+$  mode for data sample .

PDF used for signal	Double Gaussian
PDF used for background	Argus Function(one parameter fixed at 5.29)
Efficiency	9.20 %
Data yield	$1029 \pm 74$

Table 4.2: PDF's used and final results of  $M_{bc}$  fit for  $\bar{D}^0 \rightarrow K^- \pi^+$  mode.

## 4.8 Final results:

Measured R	$1.62 \pm 0.17$
R(PDG) [6]	$2.08 \pm 0.05$
Measured $\epsilon(\text{data})/\epsilon(\text{MC})$	$0.88 \pm 0.05$
True $\epsilon(\text{data})/\epsilon(\text{MC})$	1.00

Table 4.3: Final results for relative tracking efficiency of slow pions

## 4.9 Conclusions:

1. Measured relative tracking efficiency of slow pion is  $2.4\sigma (< 3\sigma)$  away from the true relative tracking efficiency.
2. Therefore, our result matches with the PDG value within error bars.
3. Errors are purely statistical.

## Chapter 5

# Details of the Silicon Vertex Detector(SVD)

The main purpose of the Belle II SVD is to determine the decay vertices of the two B mesons for CP violation measurement and also to precisely measure the momentum of charged particles.

### 5.1 SVD Outer Layout:

The layout is made of four layers of DSSD. The sensors are equipped with APV25 chips for signal readout, which are compatible with required timing and trigger tasks [7].

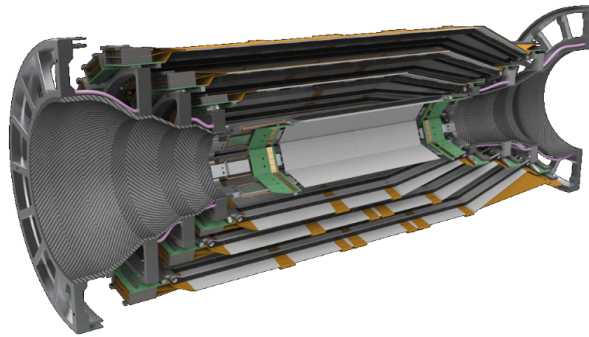


Figure 5.1: 3D view of SVD cross-section[8]

Three kinds of DSSD sensors are used in the SVD: two rectangular (large rectangular and small rectangular) and one trapezoidal (wedge sensor). The 4 layers from 3 to 6 are set at 39 mm, 80 mm, 104 mm and 135 mm from IP, and they are composed respectively of 7, 10, 12, 16 ladders. Layer 3 ladder contains 2 small rectangular sensors. Layer 4, 5 and 6 ladders contains one slanted wedge sensor in the forward region and 2,3 and 4 large rectangular

sensors respectively in its other parts. The ladders are glued into aluminium end mounts, and they are screwed on support rings on both ends of SVD, out of its acceptance. These rings are glued onto two carbon fibre cones, mounted to the end flanges. The flanges are connected with a carbon 1 mm thick fibre shell which encloses the whole VXD.

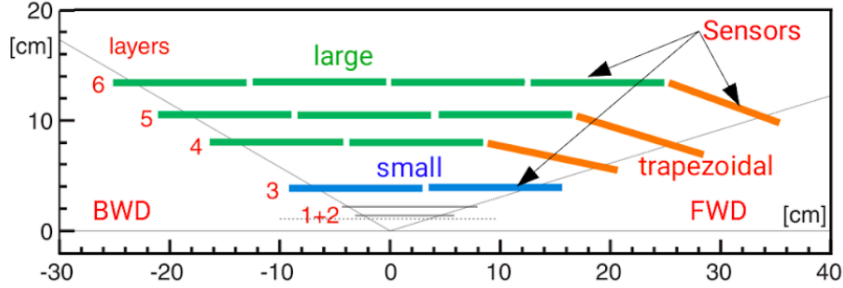


Figure 5.2: SVD layers and their sensors. [2]

The lack of symmetry of the detector on  $r - \phi$  plane for the ladder per layer number, due to sensor dimensions. The long strips of the sensors are parallel to the beam axis ( $z$  direction) on p-side. The short strips are along the  $r - \phi$  direction on the n-side, in the outward sensor face. This orientation choice is to minimize the spread of carrier during the drift due to the magnetic field interaction. The slanted forward sensors allow increasing the angular acceptance of the SVD with a reduced material budget in the forward region. This particular geometry represents a considerable challenge for ladder mount and its stability.

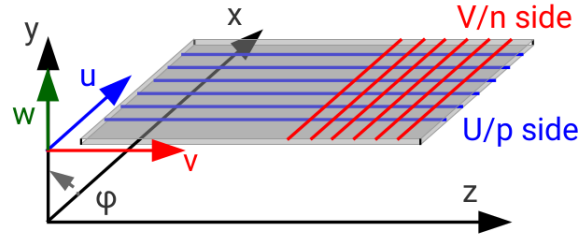


Figure 5.3: Information of 2D position coordinates. [2]

## 5.2 SVD sensors and readout electronics

The SVD sensors are Double Sided Silicon Sensors(DSSD) with 768 strips on p-side and 512 strips on nside, except for Layer 3 sensors (i.e. the small rectangular sensors) which has 768 strips on both sides.The pitch of the strips (i.e the space between consecutive strips) is different for various kind of sensors and sides, and varies from 50 m to 240 m.The large rectangular and the wedge sensors are read from 6 chips on pside and from 4 chips on nside,whereas the small rectangular sensors are read from 6 chips on both sides. All the sensors have a nominal thickness of 300 m.

## 5.3 SVD Ladders

The ladders layout is different for each layer but the mechanical support structure is same.The sensors are glued between a light-weight 1 mm thick Ariex foam layer to ensure electrical and thermal isolation.Two carbon fibre ribs are present to provide the support structure.The Layer 3 ladder consists of two small rectangular sensors with readout chips set at both ends of the ladder. The Layer 4, 5 and 6 ladders are composed of three sub-assemblies each:forward,backward and origami subassembly. The backward and the forward subassembly are composed of a single sensor, respectively a large rectangular or a wedge sensor, and of a hybrid readout sandwich.

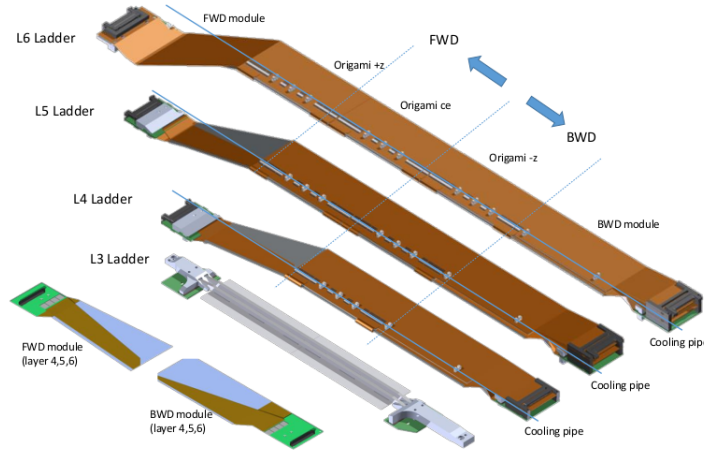


Figure 5.4: SVD ladders layout for the various layers. The Origami,sensors subdivision and the cooling pipe is higlighted. The forward and backward modules are shown separately [2].

## 5.4 Design basics of a silicon micro-strip sensors:

Silicon micro-strip sensors are composed of a few basic building blocks which can be found. This section will shed light on the design basics of a single-sided silicon microstrip sensor [7].

1. Strip implants: These are the segments of the electrode creating the electric field. Most of the field lines end at these strips, and the charge carriers drifting along the field lines induce their signal in the strips.
2. Backplane: The other side of a single-sided silicon microstrip sensor is an unstructured electrode consisting of an aluminium layer and an underlying heavily n-type doped area for preventing a Schottky contact. For a DSSD this electrode is segmented as well, and the strips consist of the same elements as on the other side, plus additional measures for strip insulation.
3. Aluminium strips: The induced signal is capacitively coupled to aluminium strips above the implanted strips to filter away the DC component of the dark current. A small part of the field lines ends at these aluminium strips.
4. Coupling oxide: This thin oxide layer is the dielectric between the implanted strips and the aluminium strips.
5. AC pad: These contact pads allow to connect the readout electronics to the aluminium strips, and serve as contact pads for sensor tests.
6. DC pad: These contact pads allow to contact the strip implants for sensor tests, and connect the bias resistors to the implanted strips.
7. Oxide windows (vias): At some points the coupling oxide has to be opened to allow contact to the silicon substrate underneath.

## Chapter 6

# Double Sided Silicon Sensors (DSSD's)

Every high energy physics experiment tracks the trajectories of the charged particles emerging out from the interaction point. Among all possibilities, silicon microstrip sensors are most suitable, thus making them the most favoured tracking sensors used in the track sensitive part of particle detectors.

### 6.1 Working Principle:

The SVD primary task is to reconstruct efficiently the B vertices and the low momentum tracks. It must be highly segmented and must have reduced readout latency to cope with the high rate and to suppress the background hits. Because of the typical low momentum of the particles, the material budget must be as low as possible. The Belle II solution to these issues has been the double-sided silicon strip detectors (DSSD).

A charged particle that crosses a silicon layer loses energy for ionization and creates an electron hole (e-h) pair. To overcome the issue of noise of intrinsic carriers, a reverse-biased p-n junction is used. In Belle II the bulk of the silicon layer is n doped and one side of the silicon layer a highly doped p implant is realized. The resulting depletion region is increased with the application of a bias voltage  $V$  bias that produces an inverse polarization on the p-n junction. Since inside the depleted region the intrinsic carriers are removed, the e-h pairs produced by charged particles become detectable. Because of the electric field produced in the junction, they can drift to the edge of the depleted region, where the charge collection electrodes are located. The DSSD sensor is segmented with p+ implant strips on one side and on the other side with n+ implant strips. Both are kept orthogonal to each other. Then on top of each strip (on both sides) an aluminium strip electrode is capacitively coupled. With this configuration, the e's drift to the n+ strips and the h's drift to the p+

strips .They induce a signal at the nearest electrode. The capacitive coupling is realized typically with an oxide layer between the metallic strip and the doped silicon one. Another expedient is the realization of a p doped implants between the n + strips (called p-stop),to avoid electrical conduction between adjacent strips.

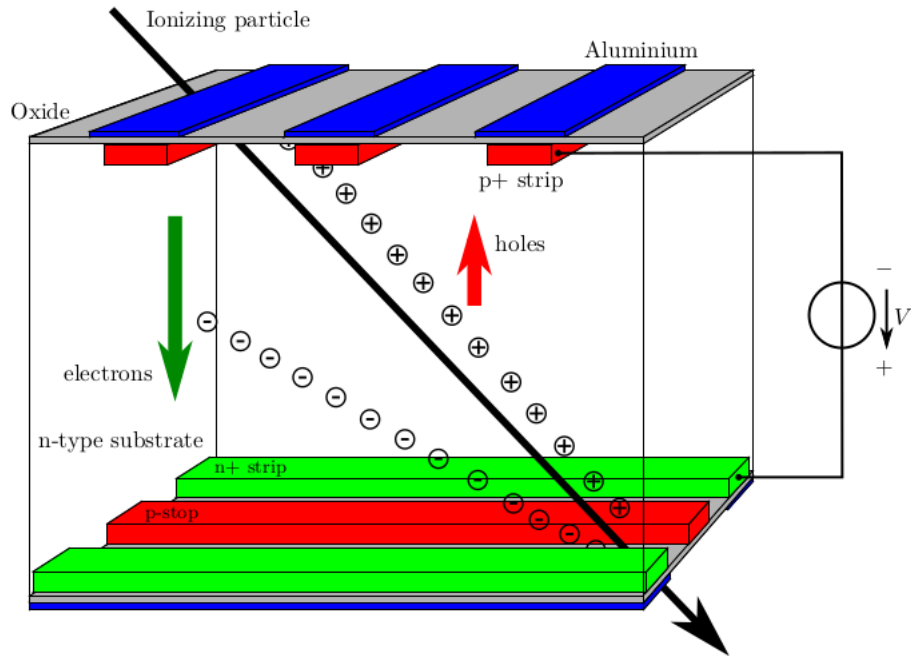


Figure 6.1: A cross section of DSSD with the operating principle.[2]

## Chapter 7

# Electrical Test Procedures

The electrical active components are tested after their manufacture to check the correct functionality and to identify possible defects. These defects, in general, are not visible from a mechanical test or optical survey.

The electrical tests are usually performed in clean rooms in a controlled environment maintaining temperature and humidity, at a test-stand equipped with the given instrumentation:

1. A black-box that maintains optical isolation of the device under test. An integrated sensor measures the temperature of the test-environment during the procedure.
2. A data acquisition system (APVDAQ) which is based on VME hardware and Lab-View software.
3. High voltage power supplies, provide bias voltage up to 200 V to the subassembly.
4. Low voltage power supplies the acquisition board and to generate the needed power (-5 V to +5 V) required by the APV25.
5. A board is used that to provide an additional potential difference  $V_{sep}$  between the chip and the bias ring, from -5 V to +5 V.

The equivalent circuit of the DSSD with the power supply and readout scheme is shown below. The bias voltage of 100 V is applied symmetrically on two sides with respect to ground through the Bias rings and R bias. APV25s are biased as 1.25 V and 2.5 V with respect to the sensor side, to provide the correct operating voltage. The potential difference through the coupling capacitor is made as small as possible to limit the stress on the delicate oxide layer which can easily break causing defects, called pinholes. When pinholes are present an undesirable DC current flows into the APV25 and an additional  $V_{sep}$  voltage is provided to tune the reference of chips.



**Pinhole:**

A breakdown of the oxide layer between the aluminium electrode and the strip implant, mostly on the p-side. The result is a flow of current from the implant, through the defects, towards the chip (instead of R bias), if a potential difference between the strip and the APV25 is present. [7] This effect saturates the amplifier and makes it unusable, thus reducing its gain. Therefore a pinhole is identified by a low gain, and from a gain variation in function of  $V_{sep}$ . It peaks at a precise value, ( $V_{sep} = 0.75$  V), with a maximum which is similar to the natural expected value, and a lower gain for all other  $V_{sep}$  values. The gain is lower because of the current flowing through the pinhole, but if the voltage drop crossing  $C_{AC}$  vanishes, the pinhole current disappears and the gain of the strip is restored. 0.75 V is the natural voltage drop across  $C_{AC}$  due to the input voltage on the APV25, thus this feature allows to cure the pinhole setting the  $V_{sep} = 0.75$  V for all the defective sensor.

**Noisy:**

A strip shows a noise level higher than expected. Most of noisy strips are due to another defect (open, short, pinhole), but some strips do not show the feature of these defects but still result noisy.

# Chapter 8

## Software Setup:

The most common defects that can be identified from the tests along with their electrical features were described in the previous chapter. The defects are automatically found and classified with a dedicated software that uses the combined result of the tests.

### 8.1 Package Content:

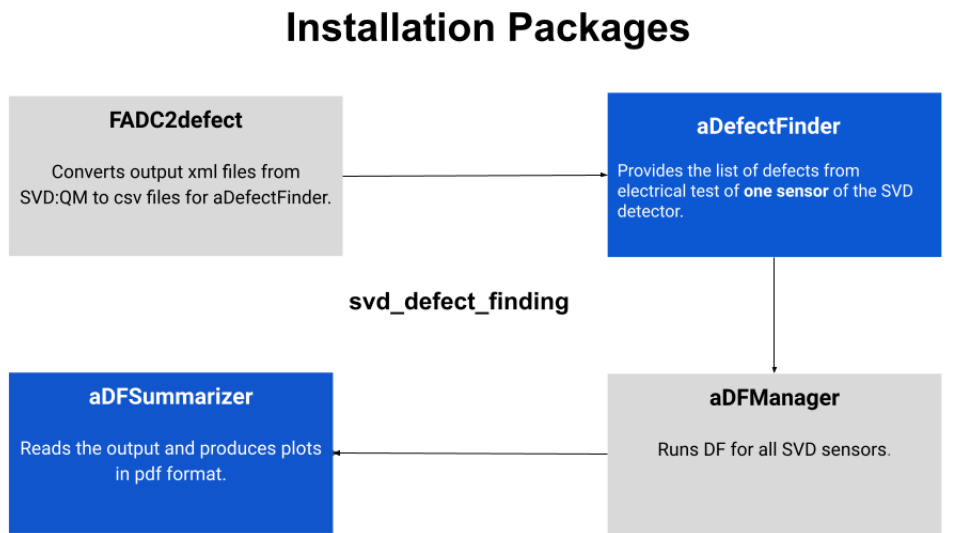


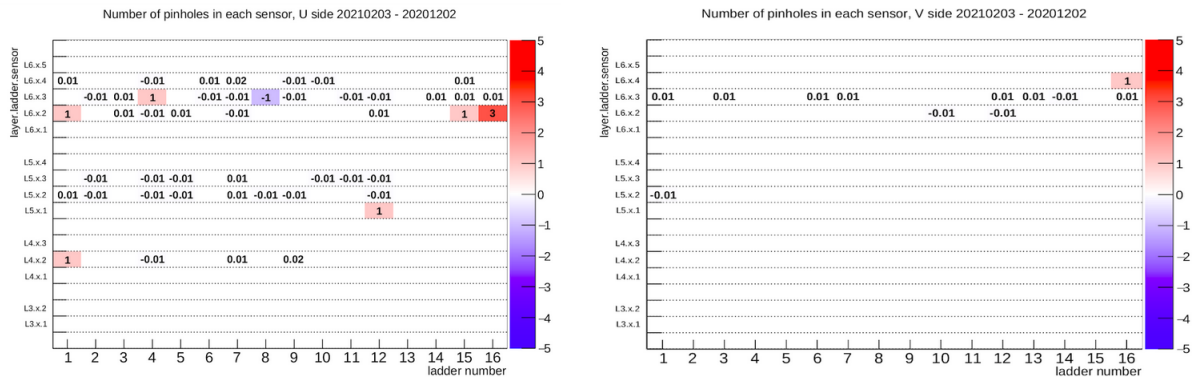
Figure 8.1: Software packages used (in order)

# Chapter 9

## SVD aDefectFinder analysis

### 9.1 aDF analysis of 2021-02-03 run; Exp 15, Run 285

Sensors with an increase/decrease in pinhole count with respect to reference run (2020-12-02):



#### Inference:

1. The plot shows increase/decrease in the number of pinholes with respect to the reference run(2020-12-02).
2. The blue shade indicates decrease in pinholes whereas the red indicates increase.
3. The defective strips at the edge of sensors (0,1,2,3...509,510,511 or 765,766,767, depending on the sensor) are counted as 0.01.
4. Therefore if we get a number like 1.01 it indicates:1 pinhole increase in the edge sensors(+0.01) and 1 pinhole increase in the non edge sensors(+1).

Let us consider defective sensor L6.8.3. Complete analysis of this sensor is shown in this section. Other defective sensors are also analysed similarly.

We first check the summary sheet obtained from the aDFManager package. From the summary sheet, we observe a difference for strip 29 of U side. In order to realize whether it is a real pinhole or not, we check their respective plots.

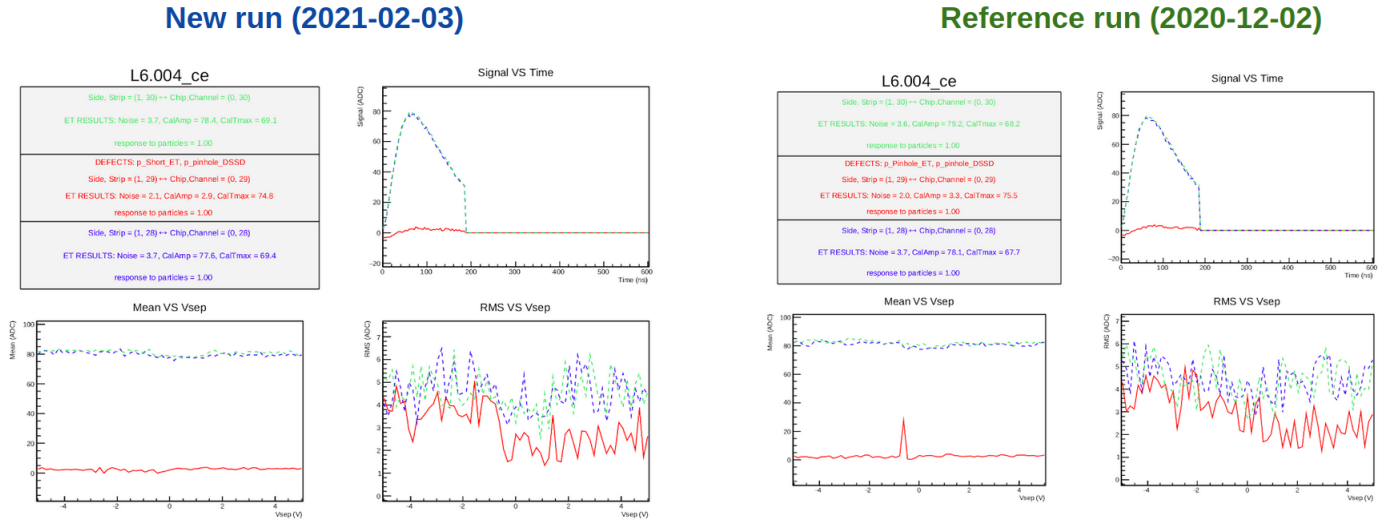


Figure 9.1: Comparison of 2021-02-03 run plot with respect to 2020-12-02 run

Since a pinhole peak is observed in the reference run and not in the new run, therefore we conclude for sensor L6.8.3 : Real DSSD pinhole rightly identified as a pinhole in reference run and wrongly identified as short in new run (low gain).

Similarly we conclude for other defective sensors as well.

Format: Side, Strip(chip, channel): Type

### Final Conclusions:

Format-Sensor: Increase/Decrease in defects: Side, Strip: Type

1. 6.1.2: +1:1,24: Real DSSD pinhole rightly identified in the new calibration and wrongly identified as short in the old (low gain)
2. 6.4.3: +1:1,602: New calibration wrongly identifies noisy strip to be pinhole. Reference calibration rightly identifies.
3. 6.15.2: +1:1,480: Real DSSD pinhole identified rightly in the new calibration and wrongly identified as short in the old (low gain).
4. 6.16.2: +3:1,309; 1,311; 1,527: Real DSSD pinhole rightly identified in the new calibration and wrongly identified as short in the old (low gain).

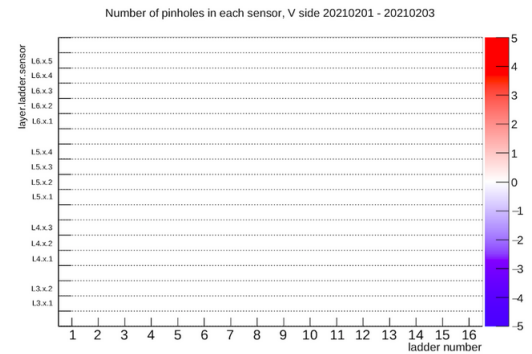
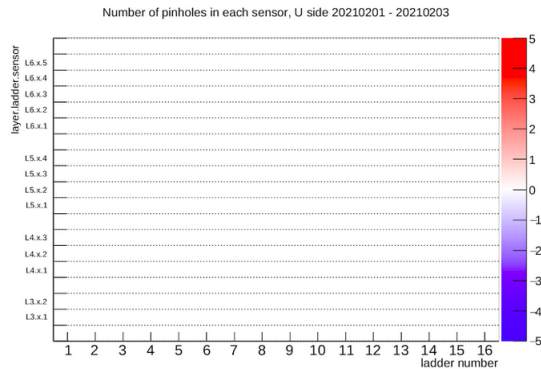
5. 4.1.2:+1:1,20: Real DSSD pinhole rightly identified in the new calibration and wrongly identified as short in the old(low gain).
6. 5.12.1:+1:1,418: New calibration rightly identifies pinhole.Old calibration wrongly identifies it to be short.
7. 6.16.4:+1:2,162: New calibration wrongly identifies open defect to be pinhole.Old calibration rightly identifies open defect.
8. 6.8.3:-1:1,29: Real DSSD pinhole rightly identified in the old calibration and wrongly identified as short in the new(low gain).

## 9.2 aDF analysis of local run with $V_{sep}=-0.8V$ (taken on Feb 1) + vsep scan (taken on Feb 3);Exp 15,Run 223

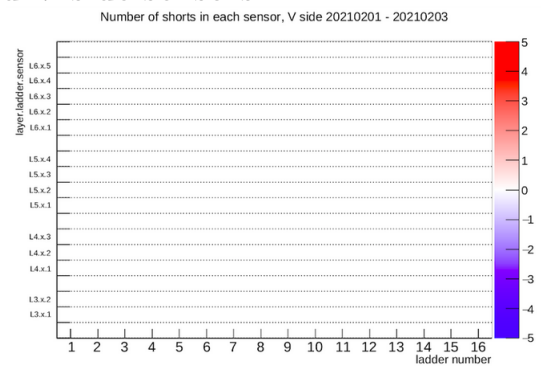
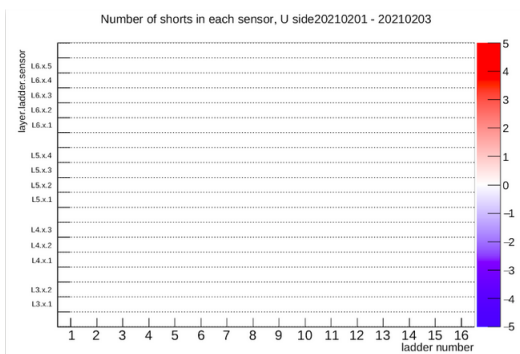
### Goal:

1. To verify if the pinhole identification is same for both runs as both are based on the same  $V_{sep}$  scan data.
2. In that case,in future we can simply take the  $V_{sep}$  scan data + some standard local run with  $V_{sep}=-0.8V$ .This will help us to avoid the additional time for intermediate local run with  $V_{sep}=0V$ .
3. This test is important to see if we can reduce the time to take the needed data for aDF during operation.

### Number of pinholes for U and V side sensors

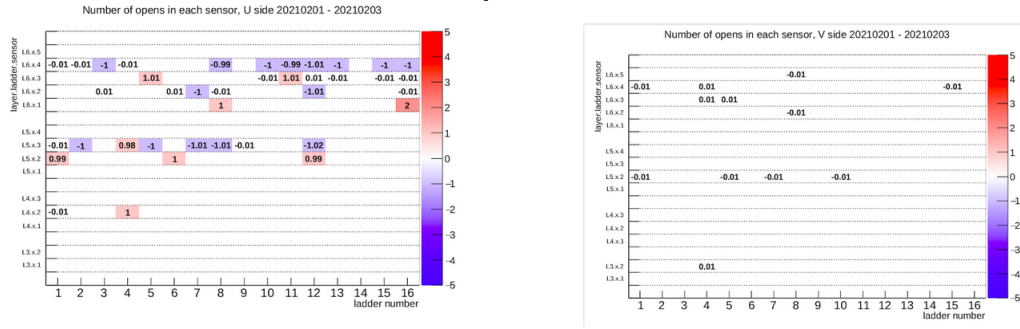


### Number of short defects for U and V side sensors

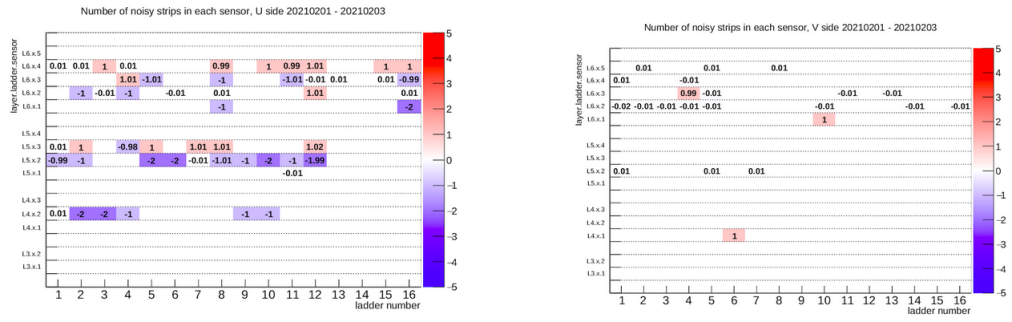


In both 2021-02-01 and 2021-02-03 runs data from same .adefectsep (that contains the information relevant for pinhole) has been used. Therefore the pinholes for both runs are similar. This might not be the case with the remaining two defects as different files are used for them.

## Number of open defect for U and V side sensors



## Number of noisy defects for U and V side sensors



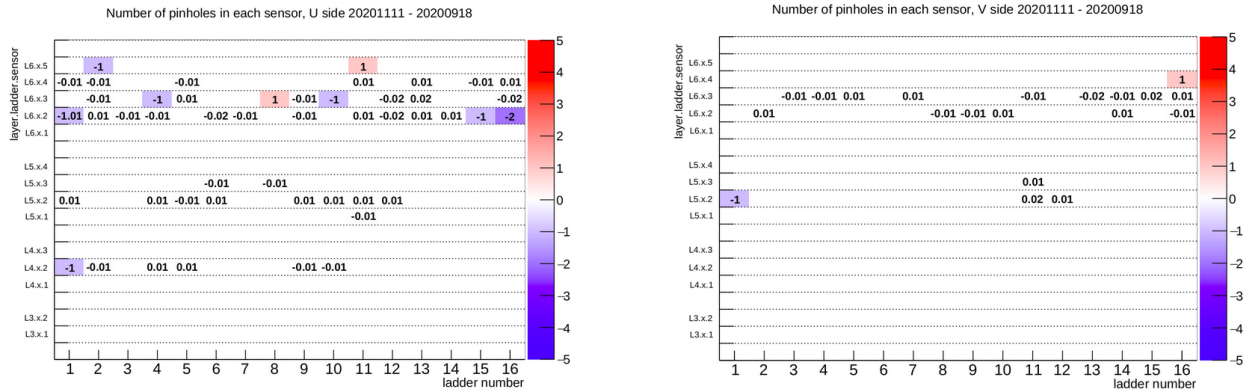
Variation observed for open and noisy defects.

### Summary for Exp 15; Run 285 and 223:

1. No pinholes observed from 2021-02-03 run.
2. Results from Feb 1 run are as expected. Therefore in future simply take the Vsep scan data + some standard local run with VSEP=-0.8V. Additional time for intermediate local run with VSEP=0V can be avoided for the future runs.

### 9.3 aDF analysis of 2020-11-11 run;Exp 14 ,Run 1028

Sensors with an increase/decrease in pinhole count with respect to reference run (2020-09-18):



#### Inference:

1. The plot shows increase/decrease in the number of pinholes with respect to the reference run(2020-09-18).
2. The blue shade indicates decrease in pinholes whereas the red indicates increase.
3. The defective strips at the edge of sensors (0,1,2,3...509,510,511 or 765,766,767, depending on the sensor) are counted as 0.01.
4. Therefore if we get a number like 1.01 it indicates:1 pinhole increase in the edge sensors(+0.01) and 1 pinhole increase in the non edge sensors(+1).

#### Final Conclusions:

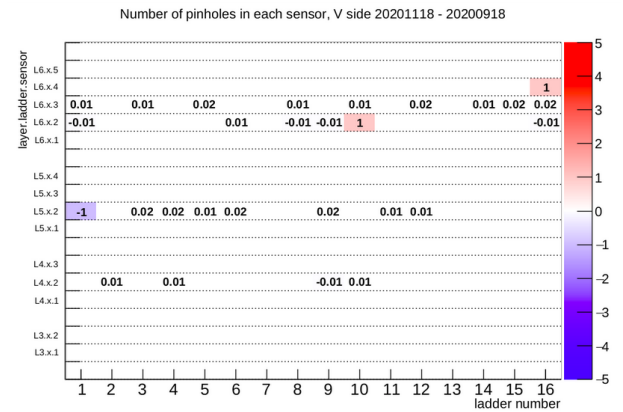
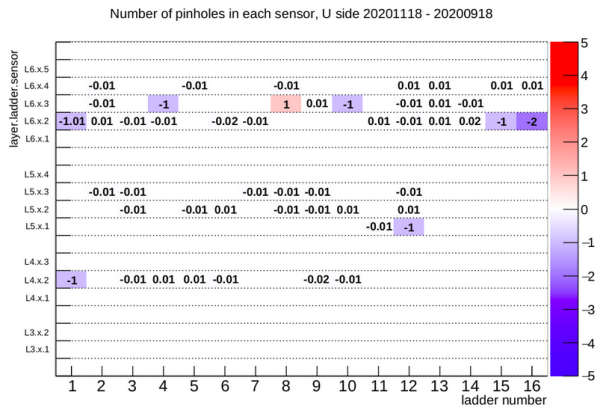
1. L5.1.2:-1:2,476 :New calibration rightly identifies Open defect.Reference calibration wrongly identifies an Open defect to be a Pinhole.
2. L6.1.2: -1:1,24 :New calibration wrongly identifies real DSSD Pinhole to be Short(low gain).Reference calibration identifies correctly.
3. L6.2.5 :-1:1,104 :Reference calibration wrongly identifies Noisy strip to be pinhole.New calibration identifies defect correctly.
4. L6.4.3 :-1:1,602:Reference calibration has identified pinhole wrongly.New calibration rightly identifies it to be a noisy strip.

5. L6.8.3:+1 :1,29:Real DSSD pinhole correctly identified in the new calibration and wrongly identified as short in the old calibration(low gain).
6. L6.10.3 :-1:1,742:Real DSSD pinhole rightly identified in the old calibration and wrongly identified as short in the new(low gain).
7. L6.11.5:+1:1,684:New calibration wrongly identifies open to be pinhole.Reference calibration correctly identifies defect to be Open.
8. L6.15.2:-1:1,480:Real DSSD pinhole correctly identified in the old calibration and wrongly identified as short in the new calibration(low gain).
9. L6.16.2:-2:1,309;1,311:(1,309) and (1,311) Real DSSD pinhole correctly identified in the old calibration and wrongly identified as short in the new calibration(low gain).

**Thus we conclude presence of no new pinholes.**

## 9.4 aDF analysis of 2020-11-18 run;Exp 14,Run 1241

Sensors with an increase/decrease in pinhole count with respect to reference run (2020-09-18):



### Inference:

1. The plot shows increase/decrease in the number of pinholes with respect to the reference run(2020-09-18).
2. The blue shade indicates decrease in pinholes whereas the red indicates increase.
3. The defective strips at the edge of sensors (0,1,2,3...509,510,511 or 765,766,767, depending on the sensor) are counted as 0.01.
4. Therefore if we get a number like 1.01 it indicates:1 pinhole increase in the edge sensors(+0.01) and 1 pinhole increase in the non edge sensors(+1).

### Final Conclusions:

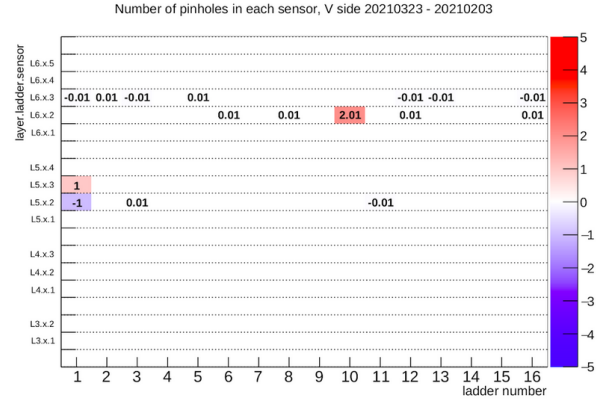
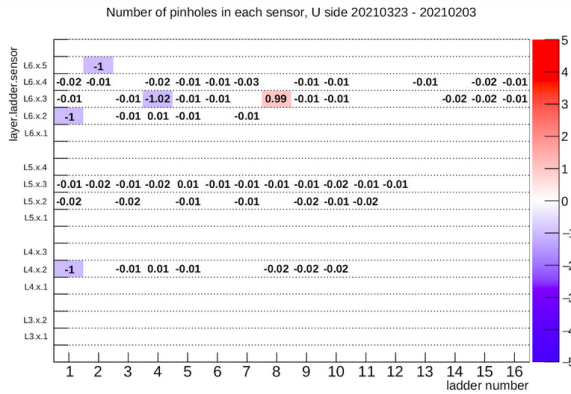
1. 5.1.2:-1:2,476:Reference calibration identifies pinhole wrongly.New calibration identifies pinhole correctly to be noisy strip.
2. 6.10.2:+1:2,508:Reference calibration identifies open defect rightly.New calibration wrongly identifies an open to be a pinhole.
3. 6.16.4:+1:2,162:Reference calibration identifies an open defect rightly.New calibration wrongly identifies open to be a pinhole
4. 4.1.2:-1:1,20:Real DSSD pinhole rightly identified in the old calibration and wrongly identified to be short in the new(low gain).

5. 6.1.2:-1:1,24:Reference calibration identifies real DSSD pinhole correctly.New calibration wrongly identifies it to be short(low gain)
6. 6.4.3:-1:1,602:Reference calibration wrongly identifies a noisy to be pinhole defect.New calibration rightly identifies noisy defect.
7. 6.8.3:+1:1,29:Real DSSD pinhole rightly identified in the new and wrongly identified as short in the old calibration(low gain).
8. 6.10.3:-1:1,742:Real DSSD pinhole rightly identified in the reference calibration and wrongly identified as short in the new(low gain).
9. 6.15.2:-1:1,480:Real DSSD pinhole rightly identified in the old calibration and wrongly identified as short in the new(low gain).
10. 6.16.2:-2:1,309;1,311:(1,309) and (1,311)Real DSSD pinholes rightly identified in the old calibration and wrongly identified as short in the new(low gain).
11. 5.12.1:-1:1,418:Reference calibration rightly identifies a pinhole.New calibration wrongly identifies a pinhole to be short.

**Thus we conclude presence of no new pinholes.**

## 9.5 aDF analysis of 2021-03-23 run;Exp 16 ,Run 1168

Sensors with an increase/decrease in pinhole count with respect to reference run (2021-02-03):



### Inference:

1. The plot shows increase/decrease in the number of pinholes with respect to the reference run(2021-02-03).
2. The blue shade indicates decrease in pinholes whereas the red indicates increase.
3. The defective strips at the edge of sensors (0,1,2,3...509,510,511 or 765,766,767, depending on the sensor) are counted as 0.01.
4. Therefore if we get a number like 1.01 it indicates:1 pinhole increase in the edge sensors(+0.01) and 1 pinhole increase in the non edge sensors(+1).

### Final Conclusions:

1. 6.10.2: +2.01:2,508 New calibration wrongly identifies an open to be a pinhole.
2. 6.10.2: +2.01:2,510 New calibration wrongly identifies an open to be a pinhole.
3. 6.10.2: +2.01:2,226 Real DSSD pinhole rightly identified as open in the old calibration and wrongly identified as pinhole in the new.
4. 5.1.3: +1:2,490: New calibration wrongly identifies noisy strip to be pinhole.Reference calibration rightly identifies.
5. 5.1.2: -1:1,480: Real DSSD pinhole identified rightly in the new calibration and wrongly identified as short in the old(low gain).

6. 4.1.2: -1:1,20 Real DSSD pinhole rightly identified in the old calibration and wrongly identified as short in the new (low gain).
7. 6.1.2: -1:1,24: New calibration wrongly identifies a pinhole to be short defect. Reference calibration rightly identifies.
8. 6.2.5: -1 :1,104: New calibration rightly identifies noisy strip. Old calibration wrongly identifies it to be a pinhole.
9. 6.4.3: -1.02 :1,0 New calibration rightly identifies open defect. Reference calibration wrongly identifies it to be a pinhole.
10. 6.4.3: -1.02 :1,767 New calibration rightly identifies open defect. Reference calibration wrongly identifies it to be a pinhole.
11. 6.4.3: -1.02 :1,602 New calibration rightly identifies noisy strip. Reference calibration wrongly identifies it to be a pinhole.
12. 6.8.3: +0.99 :1,0 Reference calibration wrongly identifies a short to be a pinhole. New calibration rightly identifies.
13. 6.8.3: +0.99 :1,29 Real DSSD pinhole rightly identified in the new calibration and wrongly identified as short in the old (low gain).

**Thus we conclude presence of no new pinholes.**

# Bibliography

- [1] <https://www.belle2.org/>
- [2] SVD aDF Confluence page:  
<https://confluence.desy.de/display/BI/SVD+defect+analysis+by+aDefectFinder>
- [3] CMS Collaboration, "Measurement of Tracking Efficiency", CMS Physics Analysis Summary, CMS PAS TRK-10-002, (2010).
- [4] <https://root.cern.ch/guides/users-guide>
- [5] N.S. Ipsita, S. Patra, S. Maity, S. Bahinipati, V. Bhardwaj, A. Giri and G. B. Mohanty, "Slow-pion Relative Tracking Efficiency Studies at Belle II", BELLE2-CONF-PROC-2021-011
- [6] <https://pdglive.lbl.gov/>
- [7] Valerio Bertacchi, Development and performance of the track finder for the Belle II Vertex Detector, Universita Di Pisa, 2016.
- [8] <https://web.infn.it/Belle-II/index.php/detector/svd>